Organic Electronics 15 (2014) 711–720

Contents lists available at ScienceDirect

Organic Electronics

journal homepage: www.elsevier.com/locate/orgel

Enhancing device efficiencies of solid-state near-infrared light-emitting electrochemical cells by employing a tandem device structure

Chia-Lin Lee, Chia-Yu Cheng, Hai-Ching Su *

Institute of Lighting and Energy Photonics, National Chiao Tung University, Tainan 71150, Taiwan

ARTICLE INFO

Article history:
Received 15 November 2013
Received in revised form 25 December 2013
Accepted 1 January 2014
Available online 17 January 2014

Keywords:
Light-emitting electrochemical cells
Organic light-emitting devices
Near-infrared

ABSTRACT

Compared to near-infrared (NIR) organic light-emitting devices, solid-state NIR light-emitting electrochemical cells (LECs) could possess several superior advantages such as simple device structure, low operating voltages and balanced carrier injection. However, intrinsically lower luminescent efficiencies of NIR dyes and self-quenching of excitons in neat-film emissive layers limit device efficiencies of NIR LECs. In this work, we demonstrate a tandem device structure to enhance device efficiencies of phosphorescent sensitized fluorescent NIR LECs. The emissive layers, which are composed of a phosphorescent host and a fluorescent guest to harvest both singlet and triplet excitons of host, are connected vertically via a thin transporting layer, rendering multiplied light outputs. Output electroluminescence (EL) spectra of the tandem NIR LECs are shown to change as the thickness of emissive layer varies due to altered microcavity effect. By fitting the output EL spectra to the simulated model concerning microcavity effect, the stabilized recombination zones of the thicker tandem devices are estimated to be located away from the doped layers. Therefore, exciton quenching near doped layers mitigates and longer device lifetimes can be achieved in the thicker tandem devices. The peak external quantum efficiencies obtained in these tandem NIR LECs were up to 2.75%, which is over tripled enhancement as compare to previously reported NIR LECs based on the same NIR dye. These efficiencies are among the highest reported for NIR LECs and confirm that phosphorescent sensitized fluoresce combined with a tandem device structure would be useful for realizing highly efficient NIR LECs.

1. Introduction

Near-infrared (NIR) organic light-emitting devices (OLEDs) would be promising NIR light sources offering advantages of light weight, low power consumption and compatibility with large area and flexible substrates. Therefore, they have received much attention due to their potential applications in telecommunications, displays and bio-imaging [1]. However, sophisticated multilayer structures and low-work-function cathodes are generally required for NIR OLEDs to optimize device efficiencies, influencing their competitiveness with other solid-state NIR emitting technologies. In contrast with conventional NIR OLEDs, solid-state NIR light-emitting electrochemical cells (LECs) could possess several superior advantages. Generally, LECs require only a single emissive layer, which can be easily processed from solutions, and can conveniently use air-stable electrodes. The emissive layer of LECs contains mobile ions, which can drift toward electrodes under an applied bias. These spatially separated ions

* Corresponding author. Tel.: +886 6 3032121x57792; fax: +886 6 3032535.
E-mail address: haichingsu@mail.nctu.edu.tw (H.-C. Su).

1566-1199/$ - see front matter © 2014 Elsevier B.V. All rights reserved.
http://dx.doi.org/10.1016/j.orgel.2014.01.001

consequently induce doping (oxidation and reduction) of the emissive materials near the electrodes, i.e. p-type doping near the anode and n-type doping near the cathode [2,3]. The doped regions induce ohmic contacts with the electrodes and facilitate carrier injection, giving low operation voltages and high power efficiencies.

A few literatures about solid-state NIR LECs based on small-molecule cationic transition metal complexes (CTMCs) [4–7] and polymers containing pendant CTMC groups [8] have been reported. Nevertheless, compared with visible light-emitting CTMCs [9–24], deteriorated photoluminescence quantum yields (PLQYs) of NIR light-emitting CTMCs [4,5,7] are generally measured due to the energy gap law, which states that the nonradiative decay rates of CTMCs increase as the energy gaps decrease [11]. Furthermore, self-quenching of excitons in neat films also limits the device efficiency of NIR LECs based on neat films of CTMCs. Therefore, neat-film CTMC-based NIR LECs typically exhibited external quantum efficiencies (EQEs) lower than 0.1% photon/electron [4–8]. To improve device efficiencies of NIR LECs, NIR LECs based on phosphorescent sensitized fluorescence have been reported [25]. In phosphorescent sensitized fluorescence [25–28], both singlet and triplet excitons in the host could be harvested due to effective Förster energy transfer [29] from triplet excitons of the phosphorescent host to singlet excitons of the fluorescent guest. With well developed CTMC hosts possessing good carrier balance, commercially available efficient fluorescent ionic NIR laser dyes [30] can be conveniently utilized as guests to achieve efficient NIR electroluminescence (EL). In addition, self-quenching of excitons could be mitigated in host–guest emissive layers. As a result, the reported phosphorescent sensitized fluorescent NIR LECs exhibited EQEs of ca. 1% [25]. However, these efficiencies are still not enough for practical applications and further improving device efficiencies of NIR LECs would be required.

Recently, we have demonstrated tandem LECs to reach over doubled light outputs and device efficiencies by stacking two single-layered LECs via a thin connecting layer [31]. A similar approach employing a thin metal interlayer to produce tandem white light emitting devices was also reported recently [32]. It would be a simple way to enhance device efficiencies of phosphorescent sensitized fluorescent NIR LECs. In this work, we report tandem phosphorescent sensitized fluorescent NIR LECs based on emissive layers containing a phosphorescent CTMC host doped with a fluorescent ionic NIR dye. To clarify effects of emissive-layer thickness on device performance, tandem NIR LECs with various thicknesses are studied. Output EL spectra of tandem NIR LECs can be modified by adjusting the thicknesses of the emissive layers due to altered microcavity effect. Furthermore, improved device lifetimes are found in thicker devices due to reduced exciton quenching near electrodes. The peak EQE obtained in these tandem NIR LECs is up to 2.75%, which is over triple of that achieved in single-layered NIR LECs based on the same NIR dye [25]. The device efficiencies achieved are among the highest reported for NIR LECs and thus confirm that phosphorescent sensitized fluoresce combined with a tandem device structure would be useful for realizing highly efficient NIR LECs.

2. Experiment section

2.1. Materials

The host complex (**1**) used in the emissive layer of the NIR LECs was $Ru(dtb\text{-}bpy)_3(PF_6)_2$ (where dtb-bpy is 4,4′-ditertbutyl-2,2′-bipyridine) [33]. The ionic NIR dye 3,3′-diethyl-2,2′-oxathiacarbocyanine iodide (DOTCI), which has been reported as an active material in efficient NIR dye lasers [30], was utilized as the guest material doped in the host. $Ru(dtb\text{-}bpy)_3(PF_6)_2$ and DOTCI were purchased from Luminescence Technology Corp. and Sigma–Aldrich, respectively, and they were used as received.

2.2. Photoluminescent characterization

Photoluminescence (PL) characteristics of DOTCI in ethanol were recorded at room temperature using 10^{-5} M solutions. The neat film of complex **1** for PL studies was spin-coated at 3000 rpm onto a quartz substrate using acetonitrile solution with a concentration of 80 mg mL^{-1}. The thickness of the spin-coated neat host film was ca. 250 nm, as measured using profilometry. UV–Vis absorption and PL spectra were obtained with a Princeton Instruments Acton 2150 spectrophotometer. The exciting wavelengths of DOTCI in ethanol and neat film of complex **1** are 650 and 450 nm, respectively.

2.3. LEC device fabrication and characterization

Indium tin oxide (ITO)-coated glass substrates were cleaned and treated with UV/ozone prior to use. A thin poly(3,4-ethylenedioxythiophene):poly(styrene sulfonate) (PEDOT:PSS) layer (30 nm) was spin-coated at 4000 rpm onto the ITO substrate in air and was then baked at 150 °C for 30 min. For the single-layered devices (**S1**, **S2** and **S3**), the emissive layers were then spin-coated at 3000 rpm from the mixed acetonitrile solutions of complex **1** and DOTCI (weight ratio of complex **1** and DOTCI = 99:1). The concentrations of the solutions used for spin coating of the emissive layers of devices **S1**, **S2** and **S3** are 80, 150 and 220 mg mL^{-1}, respectively. The thicknesses of the emissive layers for devices **S1**, **S2** and **S3** are 250, 440 and 660 nm, respectively. For the tandem devices, the lower emissive layers were first spin-coated at 3000 rpm from the mixed acetonitrile solutions of complex **1** and DOTCI (weight ratio of complex **1** and DOTCI = 99:1) with concentrations of 80, 150 and 220 mg mL^{-1} for devices **T1, T2** and **T3**, respectively. The thicknesses of the lower emissive layers for devices **T1**, **T2** and **T3** are 250, 440 and 660 nm, respectively. The connecting PEDOT:PSS layers were then spin-coated onto the lower emissive layers at 3500 rpm. The thickness of the connecting PEDOT:PSS layers is ca. 55 nm. Finally, the upper emissive layers were spin-coated by the same procedures used for spin-coating of the lower emissive layers. After spin coating, the samples were then baked at 70 °C for 10 h in a nitrogen glove box, followed by thermal evaporation of a 100-nm Ag top contact in a vacuum chamber ($\sim 10^{-6}$ torr). Thicknesses of thin films were measured by ellipsometry. The electrical and emission

characteristics of LEC devices were measured using a source-measurement unit and a Si photodiode calibrated with the Photo Research PR-650 spectroradiometer. All device measurements were performed under constant bias voltages in a nitrogen glove box. The EL spectra were taken with a calibrated CCD spectrograph.

3. Results and discussions

PL spectra of the neat film of complex **1** and absorption/PL spectra of DOTCI in ethanol solution (10^{-5} M) are shown in Fig. 1. Neat films of complex **1** exhibit red PL centered at 635 nm. DOTCI in ethanol solution exhibits concentrated NIR PL spectra centered at 720 nm. DOTCI shows intense absorption (molar extinction coefficient > 10^4 M^{-1} cm^{-1}) at the emission band of neat films of complex **1** and consequently efficient energy transfer between complex **1** and DOTCI would be expected to be feasible. Calculated Förster radius of complex **1**/DOTCI host–guest system is ca. 4.8 nm. Large Förster radius confirms effective host–guest energy transfer due to high molar extinction coefficients of guests (DOTCI) and significant spectral overlap of host (complex **1**) emission and guest absorption. Efficient host–guest energy transfer is essential for quenching residual host emission at lower guest doping concentrations, which reduces self-quenching of excitons on guest molecules and enhances device efficiencies consequently.

The EL characteristics of the single-layered and tandem NIR LECs were measured and summarized in Table 1 for comparison. The emissive layers of single-layered devices **S1**, **S2** and **S3** (weight ratio of complex 1 and DOTCI = 99:1) exhibit thicknesses of 250, 440 and 660 nm, respectively. The tandem devices are composed of two identical emissive layers vertically connected with a thin PEDOT:PSS layer (55 nm). The thickness of each emissive layer of tandem devices **T1**, **T2** and **T3** is 250, 440 and 660 nm, respectively. All tandem devices were operated under 5 V and single-layered devices **S1**, **S2** and **S3** were operated under 2.47, 2.45 and 2.45 V, respectively, to reach similar current densities as compared to their tandem counterparts. Time-dependent EL spectra of single-layered devices **S1** (2.47 V), **S2** (2.45 V) and **S3** (2.45 V) are shown in Fig. 2a–c, respectively. As shown in Fig. 2a, predominant NIR EL emission centered at ca. 730 nm accompanied by some residual host emission was measured for device **S1**. The relative intensity of the residual host emission increased with time and remained almost unchanged after ca. 2 h. It can be explained by the energy level alignments of the host and guest molecules [34] depicted in the inset of Fig. 2a. In host–guest LECs, doped layers result in ohmic contact with electrodes and consequently facilitate carrier injection onto both the host and the guest. Thus, both exciton formation on the host followed by host–guest energy transfer and direct exciton formation on the guest induced by charge trapping contribute to the guest emission. At the early stage of operation, the doped layers have not yet well established and higher carrier injection barrier is present. Such energy level alignments favor carrier injection and trapping on the smaller-gap guests, resulting in direct carrier recombination/exciton formation on the guest. Therefore, larger fractions of guest emission were observed initially. When the doped layers are getting well established, carrier injection onto the host and subsequent host–guest energy transfer would be facilitated, resulting in enhanced host emission. More significant residual host emission was observed in thicker device **S2** (Fig. 2b). Carrier injection onto the host and subsequent host–guest energy transfer would be less preferred in a thicker device under a slightly lower bias. Therefore, significantly enhanced residual host emission in a thicker device may result from modified output EL spectrum due to microcavity effect [34,35]. Constructive interference took place at the host emission band and the increasing temporal evolution of host emission was amplified in consequence. For further thicker device **S3** (Fig. 2c), the measured EL spectra were relatively less time-dependent. In addition, the host emission was blue-shifted and the guest emission was red-shifted, resulting in a deep valley at ca. 700 nm. The spacing between the cavity modes in a rather thick device would be smaller than that in a thinner device. If the emissive layer is thick enough, it would be possible for two or more cavity modes, at which constructive interference occurs, to appear at the visible spectral region. Shifts of emission peak wavelengths and reshaping of the emission spectra confirm that the output EL spectra are modified by microcavity effect (Fig. 2c). Evolution of EL spectra due to carrier trapping effect (Fig. 2a) would not result in such wavelength shift and spectral reshaping. Since both host and guest emissions are modified by interference, the temporal evolution of the EL spectra mainly comes from moving of recombination zone in the LEC device, which affects the relative amplitudes and spectral positions of these two emission bands. Effect of carrier trapping on temporal evolution of the EL spectra is relatively minor in thicker device **S3**.

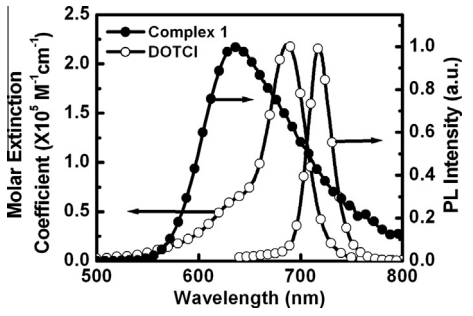

Fig. 1. PL spectra of the neat film of complex **1** and absorption/PL spectra of DOTCI in ethanol solution (10^{-5} M).

Time-dependent EL spectra of tandem devices **T1** (5 V), **T2** (5 V) and **T3** (5 V) are shown in Fig. 3a–c, respectively. The NIR EL emission of device **T1** resembled that of its single-layered counterpart (device **S1**) while device **T1** exhibited blue-shifted and narrowed residual host emission as compared to device **S1** (cf. Figs. 2a and 3a). Furthermore, enhancement of residual host emission with time was more significant in device **T1**. It reveals that for device **T1**, constructive interference occurred at ca. 600 nm and thus resulted in blue-shifted, narrowed and enhanced EL emission there. For device **T2**, the NIR EL emission

Table 1
Summary of EL characteristics of tandem NIR LECs.

Device[a]	Bias (V)[b]	J_{max} (mA cm^{-2})[c]	t_{max} (min)[d]	L_{max} (μW cm^{-2})[e]	$\eta_{ext,\ max}$ (%)[f]	$\eta_{p,\ max}$ (mW W^{-1})[g]
S1	2.47	0.36	91	5.83	1.04	6.99
S2	2.45	0.18	210	2.69	0.86	6.43
S3	2.45	0.14	402	2.56	1.14	8.16
T1	5.00	0.37	45	14.90	2.75	9.37
T2	5.00	0.17	303	6.82	2.19	8.02
T3	5.00	0.15	219	5.66	2.40	8.63

[a] Device structures of devices **S1**, **S2** and **S3**: ITO (120 nm)/PEDOT:PSS (30 nm)/emissive layer (weight ratio of complex **1** and DOTCI = 99:1)/Ag (100 nm), where the thicknesses of the emissive layers for devices **S1**, **S2** and **S3** are 250, 440 and 660 nm, respectively. Device structures of devices **T1**, **T2** and **T3**: ITO (120 nm)/PEDOT:PSS (30 nm)/emissive layer (weight ratio of complex **1** and DOTCI = 99:1)/PEDOT:PSS (55 nm)/emissive layer (weight ratio of complex **1** and DOTCI = 99:1)/Ag (100 nm), where the thicknesses of the upper and lower emissive layers for devices **T1**, **T2** and **T3** are 250, 440 and 660 nm, respectively.
[b] Bias voltage for each device to reach a similar current density.
[c] Maximal current density.
[d] Time required to reach the maximal light output.
[e] Maximal light output achieved at a constant bias voltage.
[f] Maximal external quantum efficiency achieved at a constant bias voltage.
[g] Maximal power efficiency achieved at a constant bias voltage.

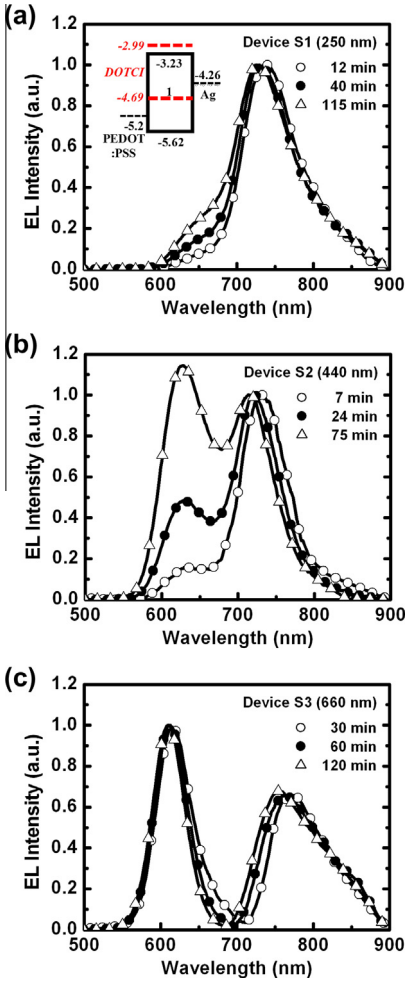

Fig. 2. Time-dependent EL spectra of single-layered devices (a) **S1** (2.47 V), (b) **S2** (2.45 V) and (c) **S3** (2.45 V). Inset of (a) energy level diagram of the host and guest molecules in the NIR LECs.

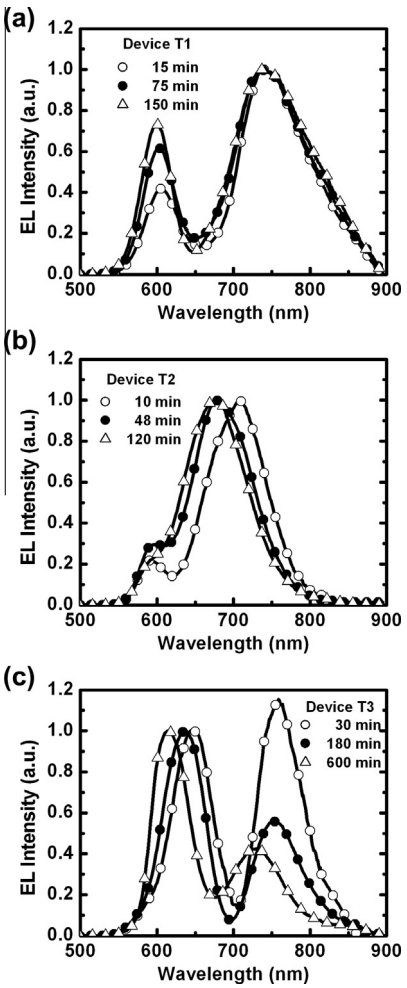

Fig. 3. Time-dependent EL spectra of tandem devices (a) **T1** (5 V), (b) **T2** (5 V) and (c) **T3** (5 V).

blue-shifted with time and the residual host emission was significantly reduced as compared to its single-layered counterpart (device **S2**) (cf. Figs. 2b and 3b). It indicates that the recombination zones of device **T2** moved with

time such that the center wavelength of constructive interference was blue-shifted. Since the blue-shifted center wavelength of constructive interference was moving toward the host emission band, the residual host emission was suppressed due to destructive interference taking place nearby the spectral region of constructive interference. For the thickest device **T3**, both the host and guest emissions were narrowed and blue-shifted with time (Fig. 3c). In addition, the relative amplitudes of the two emission bands also varied with time. Initially, both emissions exhibited comparable amplitudes (30 min, Fig. 3c) while the host emission dominated finally (600 min, Fig. 3c). In thick devices, the spacing between two cavity modes is reduced and thus both the host and guest emissions are significantly modified by interference effect. Moving of the recombination zones in device **T3** lead to shifting of cavity modes and resulted in spectral shift and alternation of relative amplitudes of the host and guest emissions consequently. These results show that the output spectra of the tandem NIR LECs are significantly influenced by the microcavity effect from device structures. The thicknesses of tandem NIR LECs should be properly chosen to obtain desired EL spectra.

Time-dependent light outputs of the single-layered and tandem NIR LECs with various thicknesses are compared in Fig. 4a–c. The peak light outputs ($\mu W\ cm^{-2}$) of tandem devices **T1**, **T2** and **T3** were enhanced by factors of 2.56, 2.54 and 2.21, respectively, when compared to those of their single-layered counterparts (devices **S1**, **S2** and **S3**, respectively) under similar current densities (Table 1). These results confirm that both the upper and lower cells connected vertically in the tandem NIR LECs contributed to output EL emission. It is noted that all of the enhancement ratios were higher than 2, which reveals that at least one of the cells in the tandem NIR LECs exhibited higher efficiencies than the single-layered device. It would arise from improved carrier balance of the lower cell when the connecting PEDOT:PSS layer was used. In previously reported time-of-flight experiments, 2,2′-bipyridine based ionic ruthenium complexes showed higher electron mobilities than hole mobilities [36]. The upper cell of the tandem device possesses the same device structure as the single-layered device, e.g., PEDOT:PSS and Ag are used for anode and cathode, respectively. When the electrochemical doped layers facilitate balanced carrier injection, the number of electrons would be higher than that of holes. Furthermore, the doped guest DOTCI, which exhibits a much lower ionization potential than the host complex **1** (the inset of Fig. 2a), would act as a hole trapper and thus further reduces the number of holes. However, when a PEDOT:PSS layer is used as the cathode, electron injection into the lower cell of the tandem device would be impeded and carrier balance is improved consequently. As shown in Fig. 5a–c, all tandem devices exhibited over doubled EQEs as compared to their single-layered counterparts. The enhancement ratios of EQEs in tandem devices **T1**, **T2** and **T3** are 2.64, 2.55 and 2.11, respectively (Table 1). These results confirm that utilizing a connecting layer with a high electron injection barrier improves carrier balance of the lower cell of the tandem device and thus the overall device efficiency of the tandem device can be higher than twice of

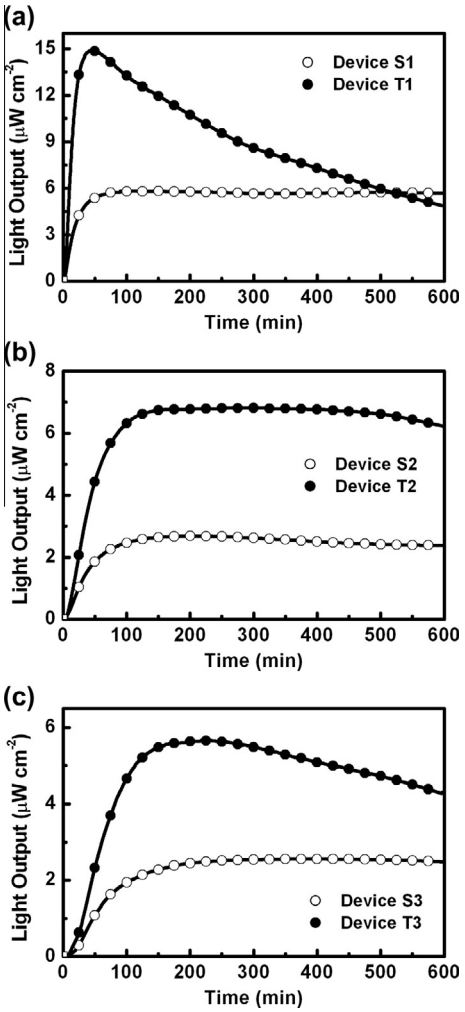

Fig. 4. Light output as a function of time for devices (a) **S1** (2.47 V) and **T1** (5 V), (b) **S2** (2.45 V) and **T2** (5 V) and (c) **S3** (2.45 V) and **T3** (5 V).

the corresponding single-layered device. Modifying device efficiencies of LECs by tailoring carrier injection efficiencies has been reported previously [37]. Even with electrochemically doped layers, the ohmic contacts for carrier injection could be formed only when the carrier injection barriers were relatively low [37]. For LEC devices with a high carrier injection barrier, e.g., electron injection at the complex **1**/PEDOT:PSS interface, the doped layers reduce carrier injection barrier but not result in a perfect ohmic contact. Therefore, the work function of the carrier injection layer would still affect carrier balance and device efficiencies.

The light outputs of the tandem NIR LECs are relatively low as compared to other reported NIR LECs. To further increase the light outputs, the constant current driving mode was tested in the tandem NIR LECs. When a constant current, which is the maximum value achieved in the constant voltage mode, was applied, the peak light outputs were enhanced by ca. 40% while the peak EQEs were reduced by ca. 15%. Furthermore, the device was turned on immediately under a constant current driving due to a high voltage applied initially. The light output increased rapidly and

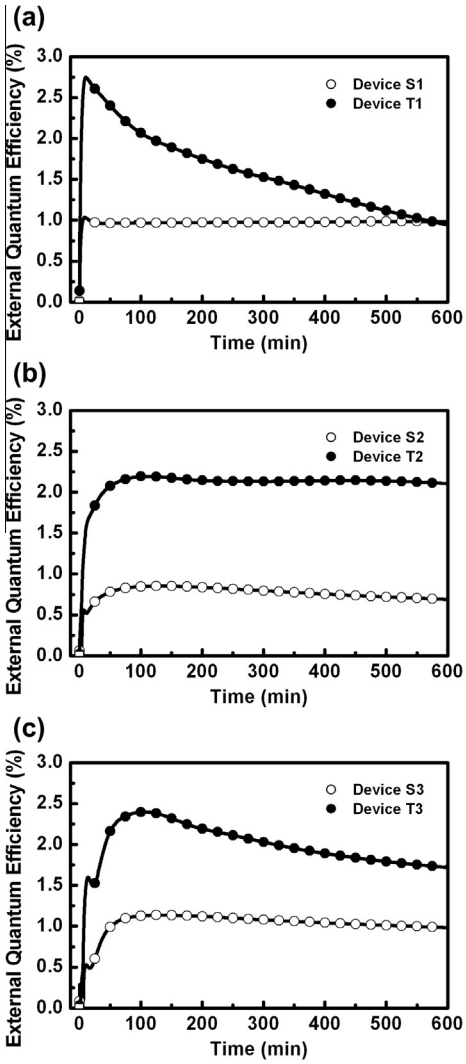

Fig. 5. External quantum efficiency as a function of time for devices (a) **S1** (2.47 V) and **T1** (5 V), (b) **S2** (2.45 V) and **T2** (5 V) and (c) **S3** (2.45 V) and **T3** (5 V).

reached the maximum within 1 min, suffering less material degradation. However, the slow increasing of light output of the LECs under constant voltage driving was accompanied by continuous material degradation and thus the peak light output was lower. Both the EQEs of the LECs under the two driving modes took place shortly after the driving was performed. Therefore, the peak EQEs of the LECs under constant voltage driving were higher due to lower initial current densities. When the tandem NIR LECs were operated under a constant current, rapid device response and higher light outputs would be obtained at the expense of lower device efficiencies.

Since the operation voltages of the tandem NIR LECs are higher than those of their single-layered counterparts, we have to examine the enhancements in power efficiencies for the tandem devices. In principle, both the light output and the operation voltage are doubled in a tandem device and thus the power efficiency (mW/W) is unchanged. However, the operation voltages of the tandem devices to achieve similar current densities are usually higher than twice of those of the single-layered devices due to the additional voltage drop across the connecting layer. It would result in reduced power efficiencies in tandem devices consequently. As shown in Table 1, we can estimate a voltage of ca. 0.1 V across the connecting PEDOT:PSS layer in the NIR tandem LECs. Nevertheless, the peak power efficiencies obtained in the tandem NIR LECs are higher than those of their single-layered counterparts (Table 1). It can be attributed to that enhanced power efficiencies resulting from additionally increased (higher than twice) EQEs owing to improved carrier balance are higher than reduced power efficiencies due to slightly increased operation voltages. The additionally increased ratios in EQEs, which are defined as the measured EQEs of the tandem devices normalized to twice of the EQEs of their single-layered counterparts, are 1.32, 1.27 and 1.05 for devices **T1**, **T2** and **T3**, respectively. These values are close to the enhancing ratios of power efficiencies of the tandem deices in comparison of their single-layered counterparts (1.34, 1.25 and 1.06, for devices **T1**, **T2** and **T3**, respectively), confirming enhanced power efficiencies due to additionally increased EQEs.

The tandem NIR LECs are designed for NIR light sources, however, some residual red host emission is present in the output EL spectrum (Fig. 3). For device **T1**, the percentage of the NIR guest emission in the total EL emission is ca. 80% (Fig. 3a). With a proper dichroic filter to selectively pass the NIR EL emission, device **T1** are still capable of offering efficient NIR EL with a peak EQE of 2.2%, which is 2.1 times the peak EQE of device **S1** and 2.75 times the peak EQE of the previously reported single-layered NIR LEC based on the same NIR dye [25]. Therefore, over doubled enhancement in device efficiency can still be achieved in a tandem device structure when only NIR emission is considered.

It is interesting to note that the device lifetime of the thinner tandem device (**T1**) was significantly shorter than that of the thicker devices (**T2** and **T3**) (cf. Fig. 4a–c). After ca. 9 h, tandem device **T1** even showed lower light outputs than single-layered device **S1** (Fig. 4a). Base on neat films of complex **1** (250 nm), deteriorated device lifetimes of tandem LECs as compared to single-layered LECs were also observed [31]. Such deteriorated device lifetimes in thinner tandem device (**T1**) would not likely result from degradation of the emissive material since no significant degradation was observed for all single-layered devices and thicker tandem devices under similar current densities during 10-h operation (Fig. 4a–c). Compared to devices **T2** and **T3**, device **T1** exhibited a higher current density (Table 1). However, no significant decay in light output under 10-h continuous operation was observed in device **S1** (Fig. 4a), which showed a similar current density as device **T1**. It reveals that degradation of the emissive material is not significant under a low current density (ca. 0.36 mA cm^{-2}). Furthermore, as shown in Fig. 6, ca. 80% current density of device **T1** retained after 10-h continuous operation while only 33% light output left finally. Hence, electrical degradation would not totally account for the decay in light output. Main degradation of light output would be related to moving of recombination zone and

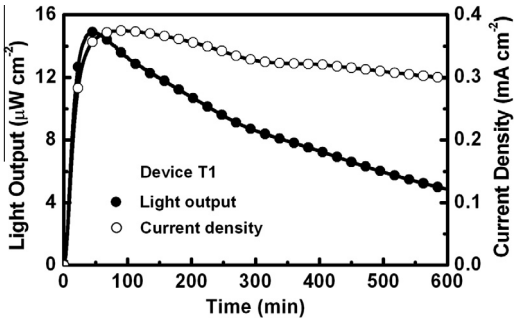

Fig. 6. Light output (solid symbol) and current density (open symbol) as a function of time for device **T1** (5 V).

subsequent exciton quenching near doped regions. Fitting of output EL spectra to simulated model concerning microcavity effect has been reported to extract temporal evolution of recombination zone in LECs under a constant bias [34]. By employing this technique, a thicker LEC was shown to exhibit larger distances between the recombination zone and the doped layers, rendering mitigated exciton quenching and enhanced device efficiency [24]. Similar methods can be adopted to study the effects of device thickness on device lifetimes of tandem LECs. The emission properties of the emissive layer can be modified in a microcavity structure and the output EL spectrum of a bottom emitting tandem LEC can be calculated approximately by using the following modified equation from Ref. [35]:

$$|E_{ext}(\lambda)|^2 = \frac{T_2\left\{c_1\frac{1}{N}\sum_{i=1}^{N}\left[1+R_1+2\sqrt{R_1}\cos\left(\frac{4\pi}{\lambda}(z_i)+\varphi_1\right)\right]+c_2\frac{1}{M}\sum_{j=1}^{M}\left[1+R_1+2\sqrt{R_1}\cos\left(\frac{4\pi}{\lambda}(L_1+L_2+z_j)+\varphi_1\right)\right]\right\}}{1+R_1R_2-2\sqrt{R_1R_2}\cos\left(\frac{4\pi}{\lambda}(L_1+L_2+L_3)+\varphi_1+\varphi_2\right)}\times|E_{int}(\lambda)|^2$$

where R_1 and R_2 are the reflectance from the cathode and from the glass substrate, respectively, φ_1 and φ_2 are the phase changes on reflection from the cathode and from the glass substrate, respectively, T_2 is the transmittance from the glass substrate, L_1, L_2 and L_3 are the optical thicknesses of the upper cell, connecting layer and lower cell, respectively, $|E_{int}(\lambda)|^2$ is the emission spectrum of the organic materials without alternation of the microcavity effect, $|E_{ext}(\lambda)|^2$ is the output emission spectrum from the glass substrate, z_i and z_j are the optical distances between the emitting sublayer i and the cathode for the upper cell and between the emitting sublayer j and the connecting layer for the lower cell, respectively, c_1 and c_2 are the emission contribution weighting factors of the upper and lower cells, respectively. The emitting layers of the upper cell and lower cell are divided into N and M sublayers, respectively, and their contributions are summed up. Since the width of p–n junction estimated by capacitance measurements when p- and n-type layers were fully established was shown to be ca. 10% of the thickness of the active layer of LECs [38,39], the emitting layer width is estimated to be tenth of the active layer thickness. Thickness of each emitting sublayer of 1 nm was used and thus N (M) = thickness of the upper cell (lower cell)/10. The PL spectrum of the structure of a tandem LEC coated on a quartz substrate was used as the emission spectrum without alternation of the microcavity effect since no highly reflective metal layer is present in this sample. Since the EL spectra of the NIR tandem LECs are composed of temporal evolution of host and guest emission due to carrier trapping effect under electrical driving (Fig. 3a), it cannot be predicted by the model of microcavity effect and would affect fitting the simulated and measured EL spectra to extract recombination zone positions. Hence, tandem LECs based on neat films of complex **1** were employed alternatively to study thickness-dependent device lifetimes.

The simulated and measured EL spectra of tandem LECs possessing thinner (265 nm) and thicker (440 nm) thicknesses of upper/lower emissive layers are compared in Figs. 7 and 8, respectively. Bias voltages of 5.15 and 5.2 V were chosen for the thinner and thicker tandem devices, respectively, to achieve similar current densities. The times at which the EL spectra were recorded and the corresponding extracted recombination zone positions are labeled on the subfigures of Figs. 7 and 8. z_1 is the distance between the cathode and the recombination zone of the upper cell while z_2 is the distance between the connecting layer and the recombination zone of the lower cell. Moving of recombination zones for the thinner and thicker tandem devices are schematically depicted in Fig. 9a and b, respectively. For each emissive layer in the thinner tandem devices, the recombination zone was initially located closer to the cathode and moved toward the anode when the doped layers were well established. The injection barrier for hole is much lower than that for electron for both the upper and lower cells of the tandem device (cf. the energy levels shown in the inset of Fig. 2a). After a bias was applied, the required number of accumulated mobile ions near the anode to achieve ohmic contact for hole was smaller than that required to achieve ohmic contact for electron at the cathode. Therefore, the hole injection efficiency was higher at the early stage of formation of electrochemically doped layers and the recombination zone would be relatively closer to the cathode consequently. When the doped layers were getting well established, balanced carrier injection could be achieved and the recombination zone would move toward the center of the active layer. After the doped layers were well established, the positions of recombination zones were relatively fixed since a stable p–i–n structure has been formed [39]. It is noted that the distances between the recombination zones and the p-type doped layers for the thinner tandem LEC reduced with time and were less than 90 nm finally (Fig. 9a). Exciton quenching in the recombination zone close to the doped layer [39] took place and resulted in deteriorated light output with time. As shown in Fig. 10, the device lifetime of the thinner

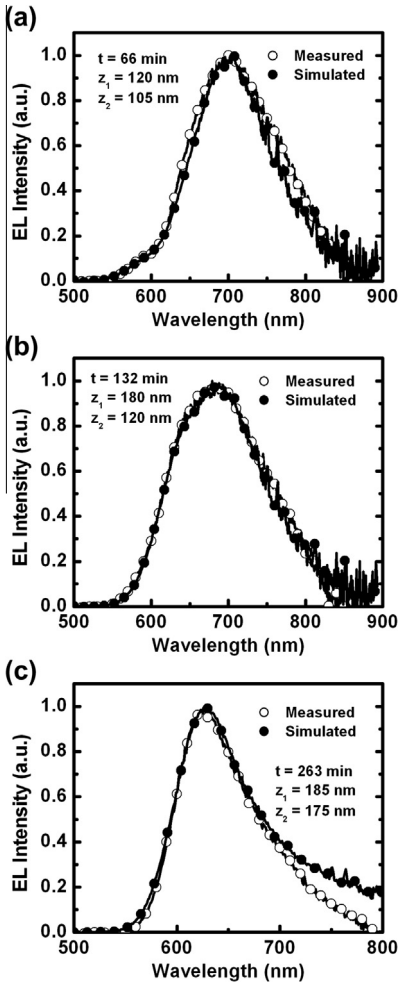

Fig. 7. Simulated (solid symbol) and measured (open symbol) EL spectra of the thinner tandem LEC (265 nm for the upper and lower cells) at (a) 66, (b) 132 and (c) 263 min after a bias of 5.15 V was applied. The extracted recombination zone positions are shown in each subfigure.

tandem LEC, defined as the time it takes for the light output of the device to decay from the maximum to half of the maximum, is only ca. 160 min. For the thicker tandem LEC under a similar bias voltage, the electric field inside the device reduced, leading to lower speed for formation of the doped layers and thus slower device response (Fig. 10). Furthermore, the number of accumulated ions near electrodes under a lower electric field would be reduced and enhancing of electron injection from cathode would be significantly affected due to a high potential barrier (the inset of Fig. 2a). Hence, the recombination zone in the upper cell of the thicker tandem LEC was relatively closer to the cathode as compared to that in the upper cell of the thinner tandem LEC (Fig. 9a and b). For the lower cell of the thicker tandem LEC, an even higher potential barrier for electron injection at the PEDOT:PSS/complex **1** interface may impede formation of the n-type doped layer under a lower bias. Slow formation and reduced thickness of the n-type doped layer near high-work-function gold cathode was also observed in planar LECs [40]. A thicker intrinsic layer, where a lower electric field is present, could thus be expected in the lower cell of the thicker tandem LEC. As the intrinsic layer shrank with time due to extension of the doped layers [39], field-dependent carrier mobilities would alter the recombination zone positions in the lower cell of the thicker tandem LEC. The electron mobilities of Ru complexes have been shown to decrease with increasing electric field [36]. Shrinking of the intrinsic layer under a constant bias resulted in increased electric field and decreased electron mobility consequently. Therefore, the recombination zone in the lower cell of the thicker tandem LEC moved toward the cathode with time (Fig. 9b). The stabilized recombination zone positions of the upper and lower cells in the thicker tandem LEC showed larger distances away from the doped layers (>170 nm, Fig. 9b). Hence, exciton quenching would be mitigated and the device lifetime of the thicker tandem LEC (ca. 270 min) was significantly longer than that of the thinner tandem LEC (ca. 160 min) under similar current densities (Fig. 10). With doped low-gap guest molecules (1 wt.%), which preferably trap holes (the inset of Fig. 2a), the recombination zones would be more closer to the anode as compared to those estimated in the host-only tandem LECs (Fig. 9). Exciton quenching near the p-type doped layers would be more severe in the thinner tandem host–guest devices due to short distances between the recombination zones and the p-type doped layers (Fig. 9a). For the thicker tandem host–guest devices, relatively longer distances between the recombination zones and the p-type doped layers would reduce exciton quenching and longer device lifetimes would be rationally expected.

In our previous published work [34], we estimated the temporal evolution of recombination zone in single-layered LECs by employing microcavity effect and attributed the reduced device efficiency to exciton quenching when the recombination zone is approaching the doped layers. By utilizing similar procedures, we studied the temporal evolution of recombination zone in tandem LECs and found that deteriorated device lifetimes also result from exciton quenching in the recombination zone near the doped layers. For the first time, these results offer direct evidence for correlating deteriorated device lifetimes with exciton quenching due to moving of recombination zone toward the doped layers. This finding reveals that brightness decay of LECs would not totally result from chemical degradation of the emissive material and proper control of recombination zone positions in LECs would be a feasible way to improve device lifetime.

Previously reported literatures about NIR LECs mainly focused on developing new NIR materials [4–8], but the device efficiencies were moderate. The main contribution of this work is proposing a combinational strategy employing existing technologies, i.e., phosphorescent sensitized fluorescence and tandem device structure, to achieve tripled enhancement in device efficiencies of the NIR LECs. Although both approaches are not new, the combination of them is undoubtedly the first demonstration. No other NIR-LEC technologies ever reported so far could offer such a high efficiency enhancement. This work is especially valuable for NIR LECs since ionic NIR materials generally suffer low efficiencies due to energy gap law. An

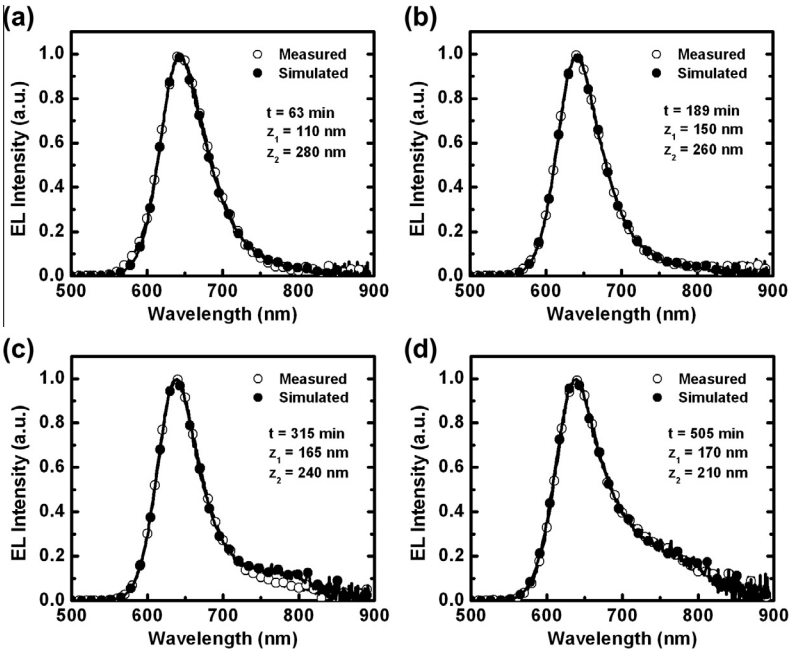

Fig. 8. Simulated (solid symbol) and measured (open symbol) EL spectra of the thicker tandem LEC (440 nm for the upper and lower cells) at (a) 63, (b) 189 (c) 315 and (d) 505 min after a bias of 5.2 V was applied. The extracted recombination zone positions are shown in each subfigure.

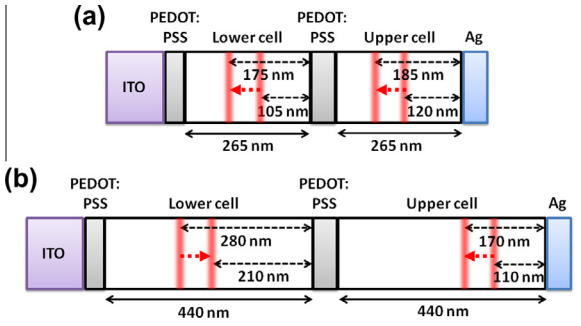

Fig. 9. Schematic illustration of moving of recombination zones in (a) the thinner tandem LEC (265 nm for the upper and lower cells) under 5.15 V and (b) the thicker tandem LEC (440 nm for the upper and lower cells) under 5.2 V.

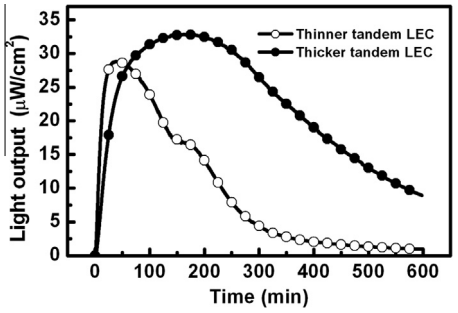

Fig. 10. Light output as a function of time for the thinner (265 nm for the upper and lower cells) and thicker (440 nm for the upper and lower cells) LECs under 5.15 and 5.2 V, respectively.

alternatively way to enhance device efficiencies by employing device technologies is necessary for this type of LECs.

4. Conclusions

In summary, we have demonstrated phosphorescent sensitized fluorescent NIR LECs in a tandem device structure. Two emissive layers containing a phosphorescent CTMC host doped with a fluorescent ionic NIR dye were connected vertically via a thin PEDOT:PSS layer. The output EL spectrum of the tandem NIR LEC was found to change as the thickness of emissive layer varies due to altered microcavity effect. In addition, by fitting the output EL spectra to the simulated model concerning microcavity effect, temporal evolution of recombination zones in the tandem LECs can be extracted. When the doped layers were well developed, the recombination zones in a thicker tandem device were closer to the center of the emissive layers while those in a thinner tandem device approached the p-type doped layers. Thus, improved device lifetimes in thicker tandem devices can be rationally attributed to reduced exciton quenching near the doped layers. The peak EQEs obtained in these tandem NIR LECs were up to 2.75%, which are over doubled as compared to those of their single-layered counterparts due to improved carrier balance induced by the connecting layer with a high electron injection barrier. Compared to previously reported single-layered NIR LECs based on the same NIR dye [25], over tripled enhancement in device efficiency was achieved in this work. These results confirm that phosphorescent sensitized fluoresce combined with a tandem device structure would be useful for realizing highly efficient NIR LECs.

Acknowledgement

The authors gratefully acknowledge the financial support from the National Science Council of Taiwan.

References

[1] G. Qian, Z.Y. Wang, Chem. Asian J. 5 (2010) 1006.
[2] Q. Pei, G. Yu, C. Zhang, Y. Yang, A.J. Heeger, Science 269 (1995) 1086.
[3] Q. Pei, Y. Yang, G. Yu, C. Zhang, A.J. Heeger, J. Am. Chem. Soc. 118 (1996) 3922.
[4] A.R. Hosseini, C.Y. Koh, J.D. Slinker, S. Flores-Torres, H.D. Abruña, G.G. Malliaras, Chem. Mater. 17 (2005) 6114.
[5] H.J. Bolink, L. Cappelli, E. Coronado, P. Gaviña, Inorg. Chem. 44 (2005) 5966.
[6] S. Xun, J. Zhang, X. Li, D. Ma, Z.Y. Wang, Synth. Met. 158 (2008) 484.
[7] H.J. Bolink, E. Coronado, R.D. Costa, P. Gaviña, E. Ortí, S. Tatay, Inorg. Chem. 48 (2009) 3907.
[8] S. Wang, X. Li, S. Xun, X. Wan, Z.Y. Wang, Macromolecules 39 (2006) 7502.
[9] J.D. Slinker, D. Bernards, P.L. Houston, H.D. Abruña, S. Bernhard, G.G. Malliaras, Chem. Commun. (2003) 2392.
[10] J.D. Slinker, A.A. Gorodetsky, M.S. Lowry, J. Wang, S. Parker, R. Rohl, S. Bernhard, G.G. Malliaras, J. Am. Chem. Soc. 126 (2004) 2763.
[11] A.B. Tamayo, S. Garon, T. Sajoto, P.I. Djurovich, I.M. Tsyba, R. Bau, M.E. Thompson, Inorg. Chem. 44 (2005) 8723.
[12] Q. Zhang, Q. Zhou, Y. Cheng, L. Wang, D. Ma, X. Jing, F. Wang, Adv. Funct. Mater. 16 (2006) 1203.
[13] H.-C. Su, F.-C. Fang, T.-Y. Hwu, H.-H. Hsieh, H.-F. Chen, G.-H. Lee, S.-M. Peng, K.-T. Wong, C.-C. Wu, Adv. Funct. Mater. 17 (2007) 1019.
[14] H.-C. Su, C.-C. Wu, F.-C. Fang, K.-T. Wong, Appl. Phys. Lett. 89 (2006) 261118.
[15] J.D. Slinker, J. Rivnay, J.S. Moskowitz, J.B. Parker, S. Bernhard, H.D. Abruña, G.G. Malliaras, J. Mater. Chem. 17 (2007) 2976.
[16] H.-C. Su, H.-F. Chen, F.-C. Fang, C.-C. Liu, C.-C. Wu, K.-T. Wong, Y.-H. Liu, S.-M. Peng, J. Am. Chem. Soc. 130 (2008) 3413.
[17] H.J. Bolink, E. Coronado, R.D. Costa, N. Lardiés, E. Ortí, Inorg. Chem. 47 (2008) 9149.
[18] L. He, J. Qiao, L. Duan, G.F. Dong, D.Q. Zhang, L.D. Wang, Y. Qiu, Adv. Funct. Mater. 19 (2009) 2950.
[19] H.-C. Su, H.-F. Chen, Y.-C. Shen, C.-T. Liao, K.-T. Wong, J. Mater. Chem. 21 (2011) 9653.
[20] C.-T. Liao, H.-F. Chen, H.-C. Su, K.-T. Wong, J. Mater. Chem. 21 (2011) 17855.
[21] H.-B. Wu, H.-F. Chen, C.-T. Liao, H.-C. Su, K.-T. Wong, Org. Electron. 13 (2012) 483.
[22] T. Hu, L. He, L. Duan, Y. Qiu, J. Mater. Chem. 22 (2012) 4206.
[23] R.D. Costa, E. Ortí, H.J. Bolink, F. Monti, G. Accorsi, N. Armaroli, Angew. Chem. Int. Ed. 51 (2012) 8178.
[24] Y.-P. Jhang, H.-F. Chen, H.-B. Wu, Y.-S. Yeh, H.-C. Su, K.-T. Wong, Org. Electron. 14 (2013) 2424.
[25] C.-C. Ho, H.-F. Chen, Y.-C. Ho, C.-T. Liao, H.-C. Su, K.-T. Wong, Phys. Chem. Chem. Phys. 13 (2011) 17729.
[26] M.A. Baldo, M.E. Thompson, S.R. Forrest, Nature (London) 403 (2000) 750.
[27] H.-C. Su, Y.-H. Lin, C.-H. Chang, H.-W. Lin, C.-C. Wu, F.-C. Fang, H.-F. Chen, K.-T. Wong, J. Mater. Chem. 20 (2010) 5521.
[28] H.-C. Su, H.-F. Chen, P.-H. Chen, S.-W. Lin, C.-T. Liao, K.-T. Wong, J. Mater. Chem. 22 (2012) 22998.
[29] T. Förster, Discuss. Faraday Soc. 27 (1959) 7.
[30] P.F. Aramendia, R.M. Negri, E.S. Roman, J. Phys. Chem. 98 (1994) 3165.
[31] J.-S. Lu, J.-C. Kuo, H.-C. Su, Org. Electron. 14 (2013) 3379.
[32] T. Akatsuka, C. Roldán-Carmona, E. Ortí, H.J. Bolink, Adv. Mater. http://dx.doi.org/10.1002/adma.201303552.
[33] S. Bernhard, J.A. Barron, P.L. Houston, H.D. Abruña, J.L. Ruglovksy, X. Gao, G.G. Malliaras, J. Am. Chem. Soc. 124 (2002) 13624.
[34] T.-W. Wang, H.-C. Su, Org. Electron. 14 (2013) 2269.
[35] X. Liu, D. Poitras, Y. Tao, C. Py, J. Vac. Sci. Technol. 22 (2004) 764.
[36] W.K. Chan, P.K. Ng, X. Gong, S. Hou, Appl. Phys. Lett. 75 (1999) 3920.
[37] C.-T. Liao, H.-F. Chen, H.-C. Su, K.-T. Wong, Phys. Chem. Chem. Phys. 14 (2012) 9774.
[38] I.H. Campbell, D.L. Smith, C.J. Neef, J.P. Ferraris, Appl. Phys. Lett. 72 (1998) 2565.
[39] M. Lenes, G. Garcia-Belmonte, D. Tordera, A. Pertegás, J. Bisquert, H.J. Bolink, Adv. Funct. Mater. 21 (2011) 1581.
[40] D. Hohertz, J. Gao, Adv. Mater. 20 (2008) 3298.